

RESEARCH

Open Access



# Deciphering cholangiocarcinoma heterogeneity and specific progenitor cell niche of extrahepatic cholangiocarcinoma at single-cell resolution

Chunliang Liu<sup>1†</sup>, Xiang Wang<sup>2†</sup>, Erdong Liu<sup>3†</sup>, Yali Zong<sup>3</sup>, Wenlong Yu<sup>2</sup>, Youhai Jiang<sup>4</sup>, Jianan Chen<sup>1</sup>, Mingye Gu<sup>5</sup>, Zhengyuan Meng<sup>5</sup>, Jingfeng Li<sup>1</sup>, Yang Liu<sup>2</sup>, Yongjie Zhang<sup>2</sup>, Jing Tang<sup>6,7\*</sup>, Hongyang Wang<sup>1\*</sup> and Jing Fu<sup>1\*</sup>

## Abstract

**Background** Cholangiocarcinoma (CCA) is a highly heterogeneous malignancy, primarily comprising intrahepatic (iCCA) and extrahepatic (eCCA) subtypes. Reconciling the variability between iCCAs and eCCAs in clinical trials remains a challenge, largely due to the inadequate understanding of their shared and subtype-specific cellular heterogeneity. We aim to address this issue using single-cell and spatially resolved transcriptomic approaches.

**Methods** We performed comprehensive single-cell RNA sequencing (scRNA-seq) by profiling 109,071 single cells from 28 samples, including chronic biliary inflammatory conditions ( $n=7$ ) and CCAs from different anatomical sites ( $n=21$ ). Findings were validated using external multi-omics datasets, tissue microarray cohort, spatial RNA in situ sequencing, CCA patient-derived organoids (PDOs), and mouse models.

**Results** iCCAs and eCCAs exhibited distinct tumor ecosystems, with notable differences in cellular composition, diversity, and abundance across various cell types. Non-malignant epithelial cells displayed divergent precancer hallmarks from different biliary sites, with inflammatory extrahepatic bile ducts exhibiting early hijacking of the gastrointestinal metaplastic process. We identified seven meta-programs within cancer cells, mapped into four major subtypes. This subtyping was validated using external CCA cohorts and PDO models, distinguishing patients based on clinical outcomes and drug vulnerabilities. Specifically, iCCAs were associated with a senescent program, while eCCAs were enriched in an IFN-responsive program linked to adverse clinical outcomes and increased drug resistance. We identified a basal-like *LY6D*<sup>+</sup> cancer cell subpopulation specific to eCCAs, which displayed significant stemness, drug

<sup>†</sup>Chunliang Liu, Xiang Wang and Erdong Liu contributed equally to this work.

\*Correspondence:

Jing Tang  
tangjingmd@hust.edu.cn  
Hongyang Wang  
hywangk@vip.sina.com  
Jing Fu  
fujing-724@163.com

Full list of author information is available at the end of the article

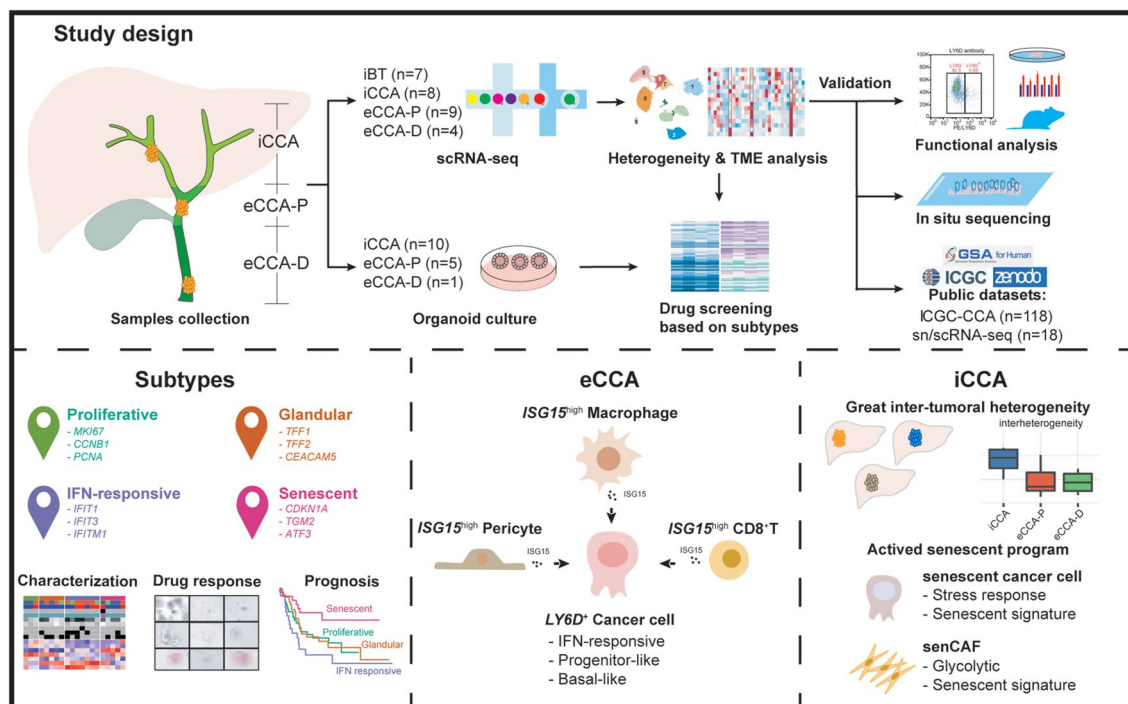


© The Author(s) 2025. **Open Access** This article is licensed under a Creative Commons Attribution-NonCommercial-NoDerivatives 4.0 International License, which permits any non-commercial use, sharing, distribution and reproduction in any medium or format, as long as you give appropriate credit to the original author(s) and the source, provide a link to the Creative Commons licence, and indicate if you modified the licensed material. You do not have permission under this licence to share adapted material derived from this article or parts of it. The images or other third party material in this article are included in the article's Creative Commons licence, unless indicated otherwise in a credit line to the material. If material is not included in the article's Creative Commons licence and your intended use is not permitted by statutory regulation or exceeds the permitted use, you will need to obtain permission directly from the copyright holder. To view a copy of this licence, visit <http://creativecommons.org/licenses/by-nc-nd/4.0/>.

resistance, and IFN-responsive features. This subpopulation was closely associated with an interferon-stimulated gene 15 (*ISG15*)-enriched mesenchymal and immune microenvironment. Functional assays demonstrated that *ISG15* stimulation significantly boosted stemness, basal-like features, and drug resistance in eCCA cells, highlighting its pivotal role in sustaining the *LY6D*<sup>+</sup> progenitor niches.

**Conclusion** We present a comprehensive single-cell landscape of CCAs, uncovering the molecular heterogeneity between iCCA and eCCA subtypes. Transcriptomic subtyping of CCA cancer cells offers implications for clinical stratification and functional precision oncology. We identify basal-like epithelial progenitors and characterize their associated *ISG15*-enriched microenvironment in eCCAs. These findings hold significant promise for the development of novel prognostic biomarkers, therapeutic targets, and treatment strategies for CCAs.

## Graphical Abstract



**Keywords** Cholangiocarcinoma, Single-cell RNA sequencing, Tumor microenvironment, Tumor heterogeneity, Basal cell, *LY6D*, *ISG15*, Epithelial progenitor

## Introduction

Cholangiocarcinoma (CCA) represents a heterogeneous spectrum of malignancies, comprising intrahepatic CCA (iCCA, 10–20%) and extrahepatic CCA (eCCA, 80–90%). The eCCA category is further subdivided into perihilar CCA (eCCA-P), and distal CCA (eCCA-D) [1]. CCA is relatively rare among gastrointestinal tract neoplasms (~3%) [2], and related clinical trials often fail to focus on specific subtypes. Recently, there is a growing recognition of the clinical, genetic, and transcriptomic disparities between CCA subtypes [1, 3]. However, the limited availability of tissues within confined anatomical regions poses the particular challenge for studying eCCAs at multi-omics levels.

Embryologically, intrahepatic small and extrahepatic bile ducts (EBTs) originate from distinct sources: the former from hepatoblasts and the latter from the caudal part of ventral foregut endoderm [4]. These bile ducts utilize canals of Hering and peribiliary gland as stem cell reservoirs, respectively [5]. Consequently, we hypothesize that different progenitor/stem cell subsets may contribute to the heterogeneity underlying CCA subtypes. Identifying these cell populations could enhance our understanding of subtype-specific cell states, tumor microenvironment (TME), and treatment response. Therefore, we endeavor to construct a single-cell atlas encompassing various CCA subtypes to decode these enigmas. We also incorporate inflammatory biliary samples to further elucidate

biliary-specific precancer hallmarks [6]. Our findings are systematically validated through External multi-omics datasets, tissue microarray cohort, spatial RNA in situ sequencing, CCA patient-derived organoid (PDO) lines, and mouse models.

## Materials and methods

### Benign and malignant human bile duct tissues

The present study received ethical approval from the Research Ethics Committees of both the Naval Medical University and the Eastern Hepatobiliary Surgery Hospital (EHBH). Informed consent was obtained from each participant. The acquisition of fresh patient samples for single-cell RNA sequencing (scRNA-seq) and PDO culture were carried out at EHBH. Detail information of patients was shown in Table S1.

### scRNA-seq and data analysis

Library preparation and sequencing were expertly handled by Shanghai Biotechnology Corporation in China using single-cell 3' v3 kits according to manufacturer's instructions (10x Genomics). Sequence reads were mapped to human reference genome GRCh38 and quantified by *Cell Ranger*. The *Seurat* and *sctransform* packages were used for data processing. Data were integrated by *Harmony*. Cells were initially annotated by classical marker genes. Gene expressing meta-programs and subtyping were analyzed by non-negative matrix factorization (NMF) method and hierarchical clustering, respectively.

### Patient-derived organoids culture and drug screening

Ten iCCAs, five eCCA-Ps, and one eCCA-Ds were collected for PDO lines establishment. A library containing 175 anti-cancer compounds was used to perform drug screening to predict therapeutic responses (Fig. 1A; Table S2). We provided more detailed description of methods in the supplementary files.

## Results

### Landscape of cellular heterogeneity between CCA subtypes

We constructed a single-cell atlas using fresh specimens from a cohort of 28 treatment-naïve patients, which spanned diverse anatomical and pathological contexts, including seven inflammatory EBTs (iBT1-7, mainly associated with cholelithiasis or choledochal cysts), eight iCCAs (iCCA1-8), nine eCCA-Ps (eCCA-P1-9), and four samples of eCCA-Ds (eCCA-D1-4) (Fig. 1A; Table S1). We profiled 109,071 cells encompassing various cell types: epithelial cells (EPCs, *EPCAM*<sup>+</sup>*KRT19*<sup>+</sup>), endothelial cells (*PECAMI*<sup>+</sup>*VWF*<sup>+</sup>), mesenchymal cells (*LUM*<sup>+</sup>*COL1A1*<sup>+</sup>), Schwann cells (*S100B*<sup>+</sup>*GAP43*<sup>+</sup>), myeloid cells (*CD163*<sup>+</sup>*CD68*<sup>+</sup>), B cells

(*CD79A*<sup>+</sup>*MS4A1*<sup>+</sup>), plasma cells (*CD79A*<sup>+</sup>*MZB1*<sup>+</sup>), T/NK cells (*CD3D*<sup>+</sup>*NKG7*<sup>+</sup>), and mast cells (*KIT*<sup>+</sup>*CPA3*<sup>+</sup>) (Figs. 1B-D, and Fig. S1). These major subsets consistently appeared across multiple samples but with uneven distribution (Figs. 1E-F). Schwann and mast cells were notably enriched in extrahepatic lesions. Tumor samples showed a pronounced infiltration of lymphocytes. Myeloid cell enrichment in iCCAs likely implied a unique Kupffer cell-associated immune niche. The desmoplastic nature of eCCA-Ps was reflected by the disproportionate distribution of epithelial and mesenchymal cells [7].

### Discriminating malignant from non-malignant EPCs and characterizing precancer cell States

We stratified EPCs ( $n=20,052$ ) into malignant and non-malignant cells using the inferCNV algorithm, identifying 20 subclones. Subclones 3, 5, and 6, predominantly from benign inflammatory bile ducts, were designated non-malignant based on low CNV scores (Figs. S2A-C). Cells with chromosomal alterations in other subclones, primarily from CCA samples, were classified as malignant EPCs, exhibiting distinct CNV profiles and salient patient occupancy (Fig. S2D).

Chronic inflammation is the hallmark of BTC oncogenesis [8], yet the precancerous epithelial states of BTCs remain poorly understood. By including samples primarily from patients with cholelithiasis or choledochal cyst, our data provides a unique opportunity to delineate the precancerous states of bile ducts, with particular relevance to BTC etiologies in East Asia [9]. We categorized non-malignant EPCs (nEPCs) into eight subtypes: gastric-like (*PGC*, *MUC6*), intestinal-like (*TFF1*, *SPINK4*), basal-like (*KRT13*, *LY6D*), mesenchymal-like (*FNI*, *VCAN*), inflammatory (*CST1*, *CXCL1/8*), immune-regulating (*SREPING1*, *HLA-A*), proliferative (*CCNB2*, *MKI67*), and developmental (*FOLR1*, *FGFR2*) (Figs. S3A, B). Pathway enrichment analysis confirmed these functional distinctions (Fig. S3C; Table S3). Gastric-like, intestinal-like, and inflammatory nEPC subtypes were more prevalent in benign inflammatory lesions, implying early hijacking of normal regenerative pathways [6]. By contrast, CNV<sup>low</sup> nEPCs within tumors were dominated by mesenchymal-like, developmental, and immune-regulating cell states, which were preferentially enriched in iCCAs, eCCA-Ps, and eCCA-Ds, respectively (Fig. S3D). These findings implied that carcinogenesis across different CCA subtypes is likely driven by differential processes such as epithelial-mesenchymal plasticity (EMP), onco-fetal reprogramming, and dysregulated immunosurveillance. By depicting the heterogeneity of precancerous epithelial states during the inflammation-carcinogenesis cascade and across the biliary tree, our data offers insights into the biliary-specific precancer hallmarks [6].

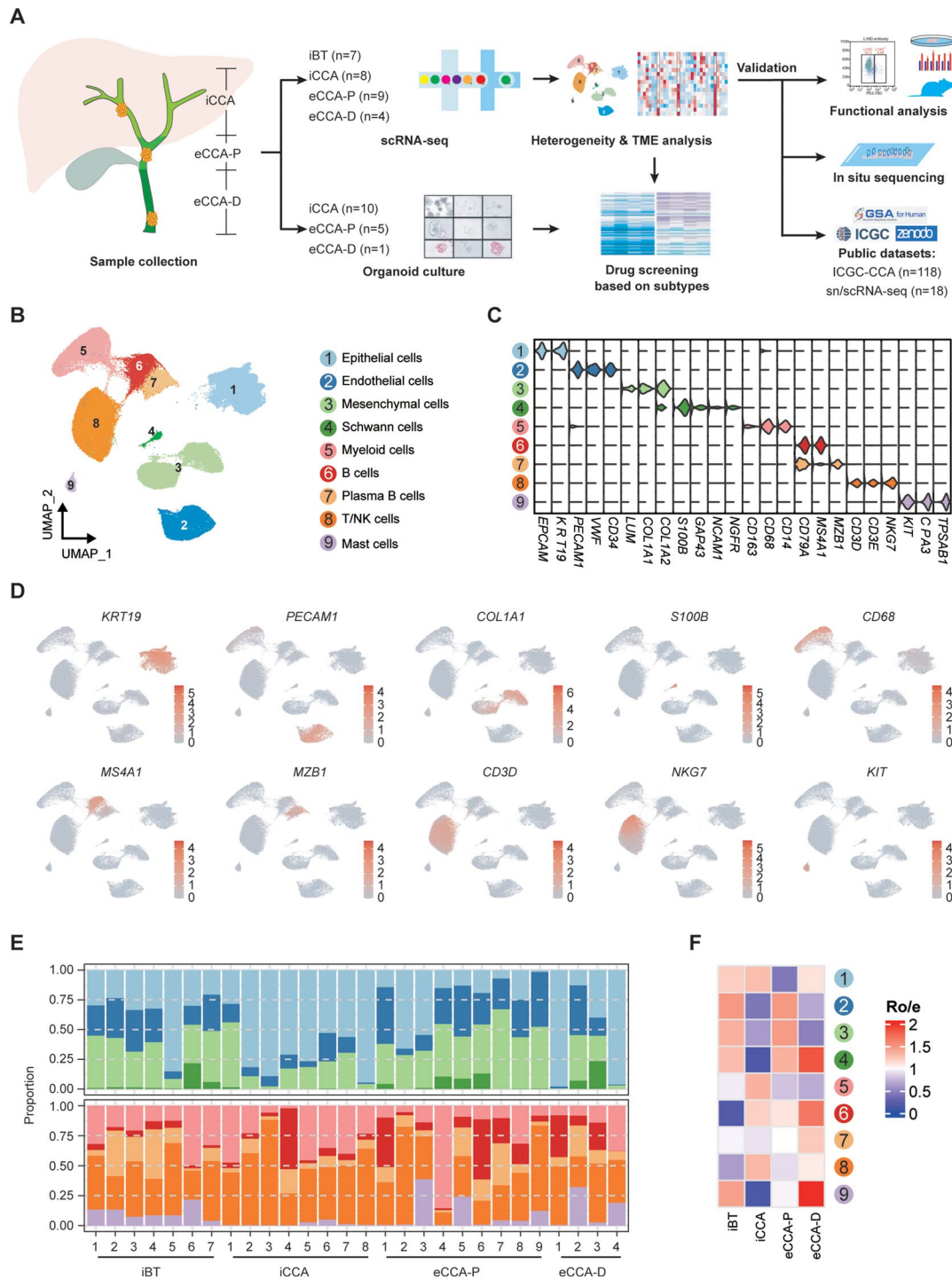


**Fig. 1** The single-cell landscape of included patients. **(A)** Experimental design and workflow of our study. **(B)** UMAP visualization of all cells from included patients colored by cell types. **(C)** Violin plot showing marker genes expression levels of each cell type. Numbers on the left side represent the cell types shown in **(B)**. **(D)** UMAP plots showing representative markers. **(E)** The proportions of nine cell types in each patient. Cell types are colored the same as **(B)**. **(F)** Sample type preference of various cell types analyzed by Ro/e. Numbers on the right side represent cell types

### Decoding shared and distinct malignant meta-programs across CCA subtypes

Next, we focused on cancer cells to explore whether different CCA subtypes exhibit shared or subtype-specific

cell states. Using the NMF method, we identified seven robust meta-programs (MPs) (Figs. 2 A and S4A; Table S4). The co-existence of mosaic MPs within individual samples highlighted significant intra-tumoral

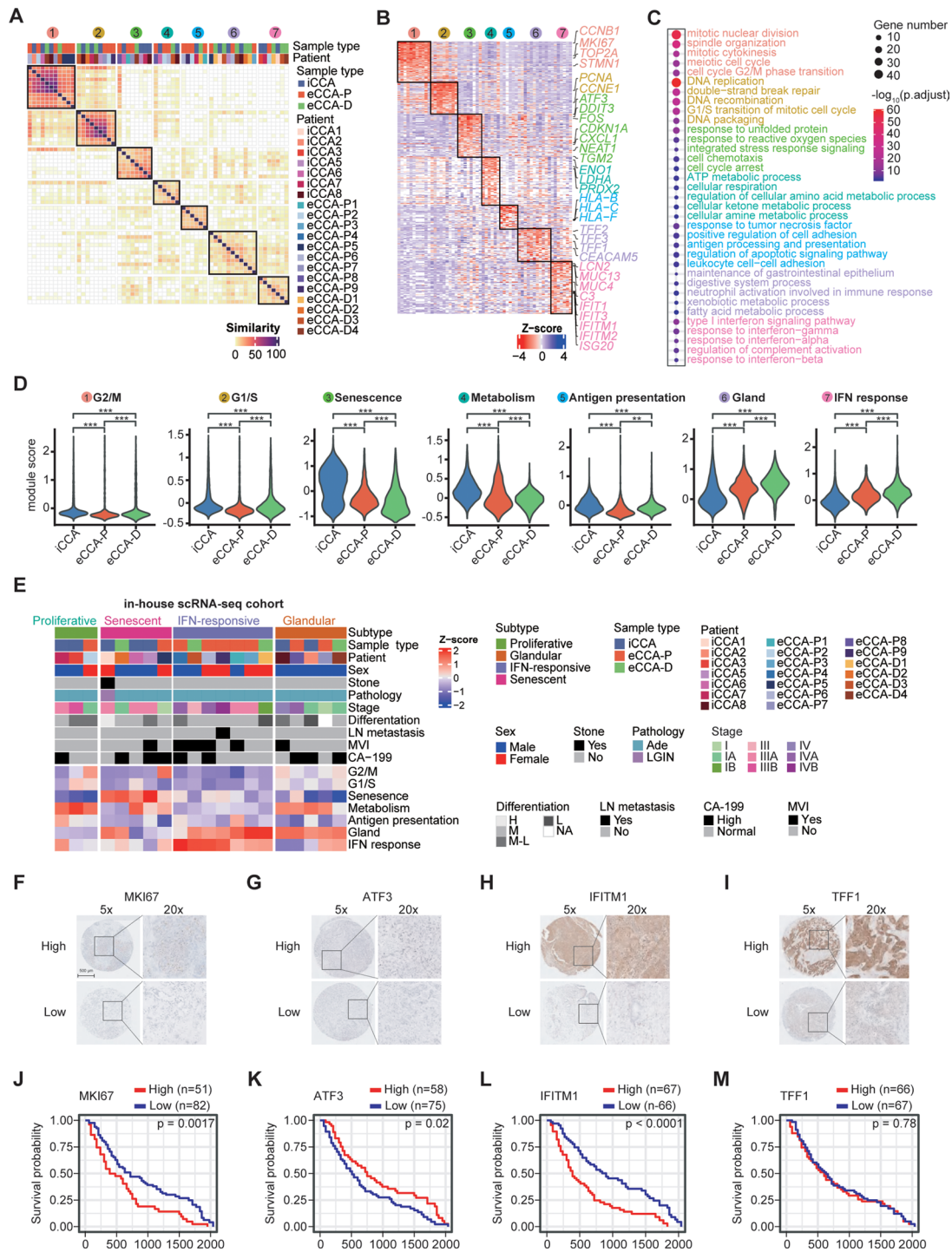


**Fig. 2** Decoding shared and distinct malignant meta-programs between CCA subtypes. **(A)** NMF analysis of mEPCs. Heatmap is colored by Jaccard similarity. Numbers on the top represent seven meta-programs. **(B)** Heatmap showing gene signatures in seven meta-programs normalized by z-score. Meta-programs are labeled the same as **(A)**. **(C)** Bubble plot showing enrichment of GO biological processes across seven meta-programs. **(D)** Violin plots comparing meta-program enrichment scores between different CCA subtypes. **(E)** Heatmap showing four subtypes of in-house CCA scRNA-seq cohort based on meta-program scores. LN, lymph node; MVI, microvascular invasion. **(F-I)** Representative IHC staining images of markers for four malignant subtypes of our CCA tissue microarray. **(J-M)** Kaplan-Meier curves comparing overall survival of four subtypes markers in our CCA tissue microarray cohort. The p values are from Wilcoxon test. \*,  $p < 0.05$ ; \*\*,  $p < 0.01$ ; \*\*\*,  $p < 0.001$

heterogeneity. These MPs were defined by specific gene modules and enriched pathways (Figs. 2B, C). MP\_01 corresponded to a generic mitotic program (G2/M), marked by *MKI67* and *TOP2A*. MP\_02, associated with the G1/S transition, featured active DNA replication (*CCNE1*<sup>+</sup>*PCNA*<sup>+</sup>). MP\_03 was linked to stress response and cellular senescence signatures, including DNA-damage-related genes (*DDIT3*, *FOS*) and cell cycle arrest genes (*CDKN1A*, *CDKN2A*), and was enriched with chemokine genes (*CXCL2/3/8*), indicative of the senescence-associated secretory (SASP) phenotype [10]. MP\_04 exhibited heightened metabolic activities with enzyme-coding genes like *ENO1* and *LDHA*. MP\_05 was associated with activated antigen-presentation pathways (*HLA-B*<sup>+</sup>*HLA-C*<sup>+</sup>). MP\_06 was enriched in glandular and mucosal defense genes (e.g., *TFF1/2/3*, *CEACAM5*). Lastly, MP\_07 presented a distinct interferon (IFN) response program, featuring IFN-stimulated genes (ISGs) such as *IFIT1/3*, *IFITM1/2*, and *ISG20*.

We further explored the distribution of these cell states across CCA subtypes by quantitatively assigning MP scores to individual cells. The senescence state (MP\_03) was predominant in iCCAs, while the gland (MP\_06) and IFN response (MP\_07) states were more prevalent in eCCAs (Figs. 2D and S4B-C). We classified each sample into MP-defined subtypes by averaging the expression of corresponding MP signatures. Hierarchical clustering identified four subtypes: proliferative (G1/S and G2/M signatures), glandular (mucosal defense and metabolism signatures), IFN-responsive (glandular and IFN-related signatures), and senescent subtype (Fig. 2E). The IFN-responsive subtype, primarily comprising eCCAs, was associated with advanced stages, lymph node metastasis, and microvascular invasion (Figs. 2E and S4D). We further explored the prognostic significance of molecular subtypes in an independent CCA cohort based on tissue microarray (TMA) data ( $n = 133$ ; Fig. 2F-M), by using subtype-specific markers (proliferative: *MKI67*; senescent: *ATF3*; IFN-responsive: *IFITM1*; glandular: *TFF1*). High expression of *MKI67* and *IFITM1* were both associated with worse prognosis, whereas increased *ATF3* expression correlated with better survival (Fig. 2J, L). Validation using the International Cancer Genome Consortium (ICGC) microarray dataset revealed similar patterns of subtype distribution (Fig. S4E-G), with the IFN-responsive subtype enriched in eCCAs and associated with advanced stages and poor prognosis (Figs. S4H, I). Collectively, these findings systematically characterize the transcriptomic heterogeneity between iCCAs and eCCAs, providing insights into CCA molecular subtypes and their clinical relevance.

### Expanding the application of molecular subtyping in functional precision oncology with PDOs

We then sought to determine whether molecular subtyping could offer therapeutic insights for precision medicine in CCAs. Given the established value of PDO models in functional precision oncology and their efficiency in large-scale drug screening [11], we leveraged our pre-established CCA PDO library to validate the molecular subtypes. We successfully established sixteen stable, treatment-naïve CCA PDOs (ten iCCAs, five eCCA-Ps, and one eCCA-D). Morphologically, these PDOs displayed thickened walls invaginating into the biliary lumens with tumor-like pleomorphic architectures. Hematoxylin-Eosin (H&E) staining validated that PDOs displayed nuclear atypia, abundant mitotic figures, and pleomorphic nuclei, faithfully preserving the malignant features of corresponding tissues (Fig. 3A). Deconvolution of the PDO bulk RNA-seq data with MP signatures revealed the predominant molecular subtype for each PDO line. Notably, the IFN-response program was enriched in eCCA PDOs, in line with our NMF-based findings (Fig. 3B).

We subsequently explored whether different subtypes could predict responses to anti-cancer therapeutics by using a library of 175 compounds, which were systematically grouped at pathway levels (Fig. S5). A proof-of-principle single concentration drug-discovery screening approach (10  $\mu\text{mol/L}$ ) was utilized for each compound. Compounds resulting in less than 50% cell viability in PDOs after treatment were considered effective [12]. High-throughput PDO drug screening revealed substantial heterogeneity of drug vulnerabilities in a personalized manner (Fig. S5). We then integrated drug screening profiles of PDOs at the subtype level (Fig. 3C), and selected the top 30 agents with the highest inhibition rate for each PDO subtype (Figs. 3D-G). These agents predominantly targeted pathways related to DNA damage response, protein tyrosine kinases, epigenetic reprogramming, and cytoskeletal signaling, which are among the most extensively studied in BTC treatment [8]. Narrowing our focus on these pathways (Fig. 3C), both in the context of the full drug panel and when analyzing the top 30 compounds, the IFN-responsive subtype consistently displayed significantly greater drug resistance. In contrast, the senescent and glandular subtypes generally exhibited increased drug vulnerability (Figs. 3D-G).

Collectively, PDO models recapitulated and validated the core biological traits and molecular subtyping of CCAs. Pharmacotyping of PDOs further advanced our understanding of phenotypic drug discovery in CCAs [13], and highlighted the potential of molecular subtyping to inform precision therapy.

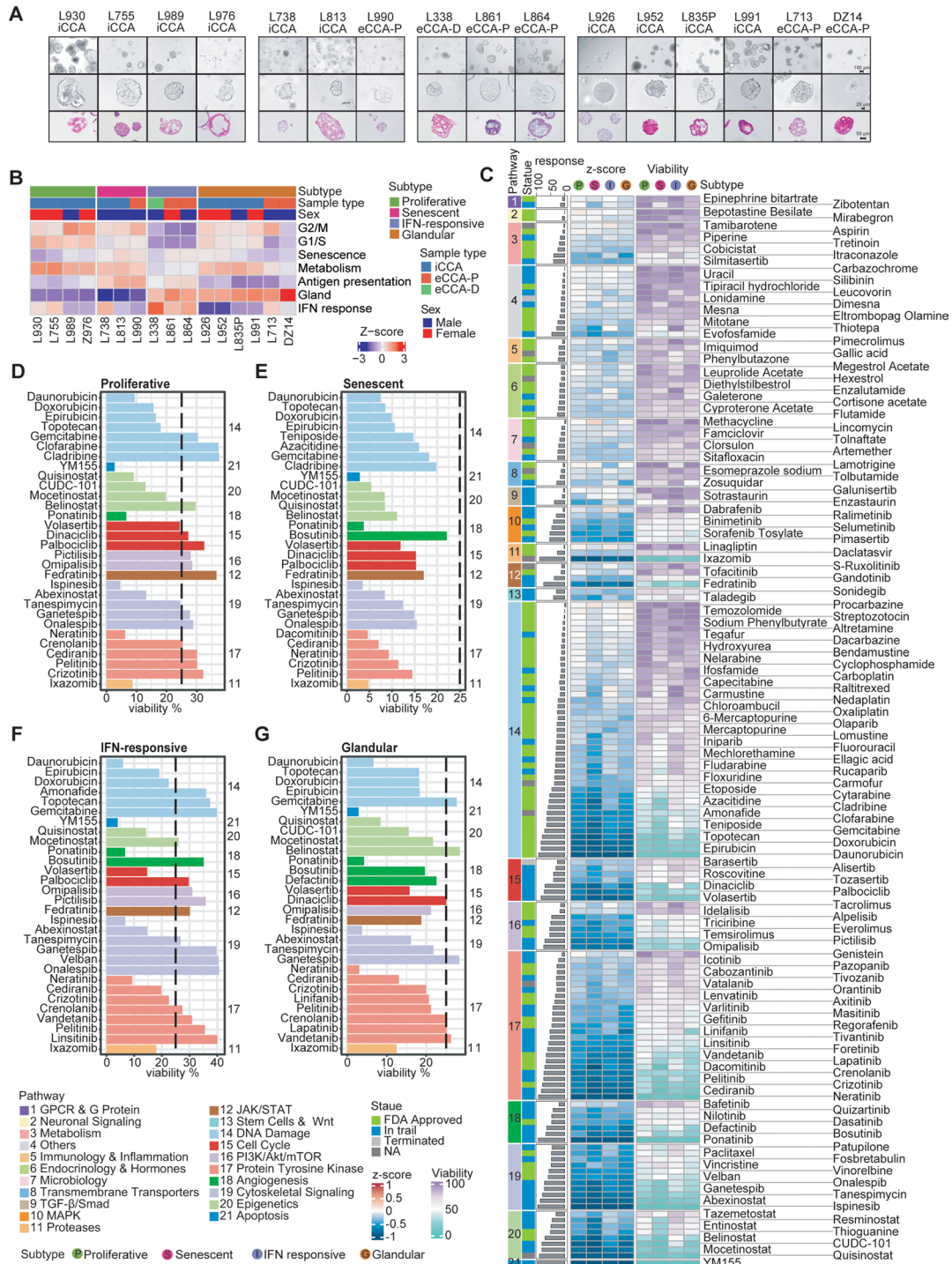


**Fig. 3** CCA subtypes recapitulated in PDO models linking to drug response. **(A)** Representative bright field and H&E staining images of 16 CCA PDOs. **(B)** Heatmap showing subtyping of 16 PDOs based on NMF meta-program scores. **(C)** Heatmaps displaying high-throughput screening of 175 drugs across four subtypes of PDOs, with the right and left side heatmap showing cell viability and normalized viability, respectively. Barplots on the left side of heatmaps showing scaled sums of z-scores representing the overall drug response. Drugs are colored by related pathways and are clustered by rows. **(D-G)** Barplot showing top 30 effective drugs in proliferative-subtype, senescent-subtype, IFN responsive-subtype and glandular-subtype PDOs

### Identifying eCCA-specific basal-like progenitor subpopulations

Beyond the functional partitioned NMF-based programs, we next asked whether distinct cancer cell subpopulations were unique for CCA subtypes. We identified 17 clusters of malignant EPCs (mEPCs), totaling 12,858 cells (cluster 0–16) (Fig. 4A; Table S5). iCCAs displayed greater inter-tumoral heterogeneity than eCCAs, but no significant difference was revealed between eCCA-Ps and eCCA-Ds (Figs. S6A–B). Several clusters were occupied by individual samples; however, a small cluster (c7) was predominantly composed by eCCAs (Figs. 4B and S6C–D). Differential gene expression (DGE) analysis revealed that c7 highly expressed basal-squamous cell markers (e.g., *KRT5*, *KRT6A*, *LY6D*, *KLK7*, *CDH3*; annotated using the Human Protein Atlas), which were also linked to development and stemness [14–16] (Figs. 4C–F). CytoTRACE analysis showed the stem-cell-like nature of this cluster (Fig. 4G). Monocle analysis demonstrated that c7 cluster initiated the trajectory and subsequently bifurcated into two branches encompassing other cancer cell lineages presumably accounting for different eCCA subtypes (Fig. 4H–I). Consistently, the expression of *LY6D*, *KLK7*, *CDH3*, *CD44*, *SOX9*, and *EPCAM* decreased along the pseudotime trajectory (Fig. 4J). Pathway analyses indicated enrichment of epidermis development/differentiation and IFN response-associated pathways in the c7 subcluster (Fig. 4K). In agreement, we observed a notably elevated score for the NMF-based IFN-response MP (Fig. S6E), further underscoring the critical role of IFN signaling in this subpopulation. To validate these findings, we leveraged three independent single-cell cohorts comprising 13 eCCAs and 5 adjacent normal tissues (ANTs) (Fig. S7A), including two scRNA-seq datasets [17, 18], and one snRNA-seq dataset [19]. Following data integration and cell annotations (Figs. S7B–E), we identified a basal-like epithelial cluster (Epi\_05) characterized by the expression of *LY6D* and *KLK7*, which was preferentially enriched in tumor samples (Figs. S7F–I). Meanwhile, Epi\_05 highly expressed multiple ISGs particularly *ISG15* (Fig. S7G). Using gene signatures based on our IFN-response MP, Epi\_05 exhibited the highest IFN-response score compared to other clusters (Fig. S7J).

We confirmed *LY6D*<sup>+</sup>*panCK*<sup>+</sup> cancer cells in eCCA samples via multicolor immunohistochemical (mIHC) staining (Fig. 5A). Employing canonical markers in scRNA-seq dataset to define major cell types (e.g., *EPCAM* and *KRT19* for EPCs), we used RNA in situ sequencing (ISS) to validate the existence of *LY6D*<sup>+</sup> cancer cells (Figs. 5B and S8A–C; Table S6), revealing higher levels of basal-like markers (*KLK7*, *KRT5*, *KRT10*), stem cell markers (*CD44*, *SOX9*, *EPCAM*), and proliferative markers (*MKI67*, *PCNA*) in *LY6D*<sup>+</sup> versus *LY6D*<sup>−</sup> cancer cells (Fig. 5C). Leveraging in vitro models, we confirmed

*LY6D* expression in the eCCA-P cell line QBC-939. FACS sorting identified *LY6D*<sup>+</sup> cells at a proportion of 6.68% (Fig. 5D). *LY6D*<sup>+</sup> cells exhibited greater spheroid formation capacity, with upregulated stem cell genes (*CD44*, *CD133*, *EPCAM*) and basal cell genes (*KLK7*, *CDH3*) (Figs. 5E, F). *LY6D*<sup>+</sup> cells also displayed enhanced resistance to gemcitabine, cisplatin and 5-fluorouracil (5-FU) (Figs. 5G), in line with the greater drug resistance of the IFN-responsive PDO subtype. Subcutaneous engraftment mice models further confirmed that *LY6D*<sup>+</sup> cells significantly generated larger outgrowth of tumors than *LY6D*<sup>−</sup> cells (Figs. 5H–I), with upregulated expression of *CD44*, *CD133* and *EPCAM* in *LY6D*<sup>+</sup> cells-generated tumors (Figs. 5J). Collectively, these results demonstrated that *LY6D*<sup>+</sup> cells behaved as eCCA-specific basal-like progenitors associated with cancer stemness and chemotherapy resistance.

### Unique mesenchymal microenvironment between different CCA subtypes

Another critical question in CCAs, archetypal desmoplastic cancers, is how cancer-associated fibroblasts (CAFs) act as key orchestrator of the TME and contribute to the stromal heterogeneity across CCA subtypes [20]. We identified 18,555 mesenchymal cells, clustering into five fibroblast subsets (c1–c5; *LUM*<sup>+</sup>*COL1A1*<sup>+</sup>) and three pericyte subsets (c6–c8; *RGSS*<sup>high</sup>) (Figs. 6A and S9A–B; Table S7) [21]. Two fibroblast clusters, benign fibroblasts (benign Fib, c1) and inflammatory fibroblasts (iFib, c2), were preferentially enriched in iBTs. The benign\_Fib highly expressed genes involved in extracellular matrix (ECM) development and remodeling, including *MFAP5* and *IGFBP6* [22, 23]. The iFib cluster exhibited elevated expression of inflammatory markers such as *C3*, *C7*, and *CCL2*, alongside activation of pathways associated with leukocyte chemotaxis and immune responses (Figs. 6B–E). The remaining three fibroblast subsets, enriched in CCAs, were classified as CAFs (Figs. 6A–C). Matrix CAFs (c3) expressed *MMP11* and *CST1* which facilitated tumor invasiveness and metastasis [24]. Stem-like CAFs (c4) were marked by stem cell markers such as *GPC3* and *SOX9*. Senescent CAFs (senCAFs, c5), chiefly residing in iCCA specimens, expressed senescence markers (*CDKN2A*, *SERPINE1*) (Figs. 6A–D) [25]. SenCAFs uniquely expressed *MCT4* and *PKM2*, both participating in glycolytic reprogramming during hepatic stellate cells (HSCs) activation and transdifferentiation towards a myofibroblast phenotype [26]. Pathway analyses validated the functional specialization of these clusters (Figs. 6E and S9C). Evidenced by the CytoTRACE transcriptional entropy, stem-like CAFs were at a less differentiated state, whereas senCAFs were oppositely at a more differentiated state (Figs. S9D, E).

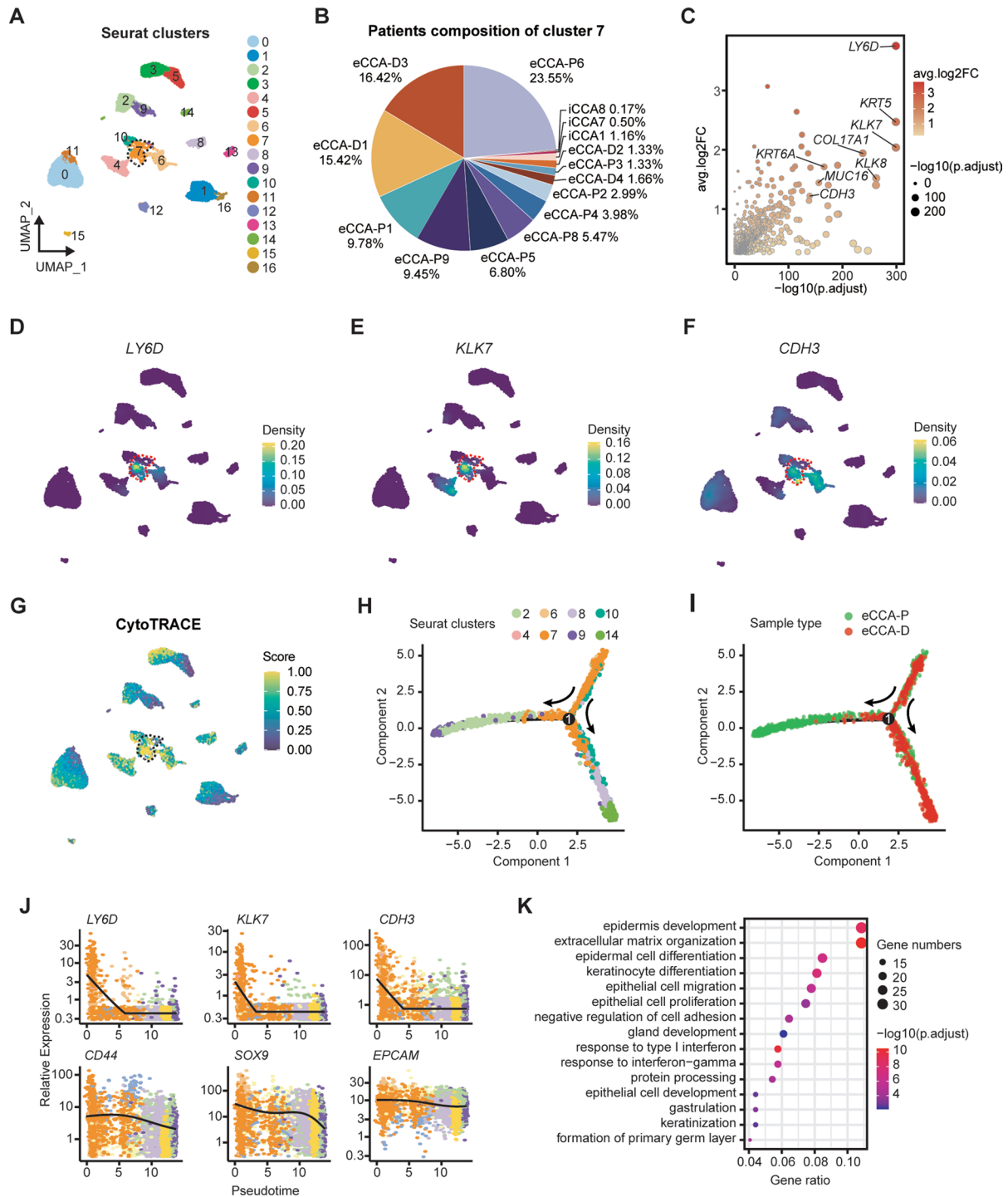


**Fig. 4** Identification of eCCA-specific basal-like progenitor populations. **(A)** UMAP plot of mEPCs colored by clusters. **(B)** Pie chart showing the patient composition of cluster 7. **(C)** Scatter plot displaying upregulated marker genes of cluster 7. **(D-F)** UMAP density plot showing *LY6D*, *KLK7* and *CDH3* expression across mEPCs. **(G)** UMAP plot showing differential transcriptional entropy of mEPCs calculated by CytoTRACE. **(H-I)** Pseudotime analysis of mEPCs from eCCA-P and eCCA-D patients. Cells are colored by Seurat clusters and sample types. **(J)** The dynamic expression of marker genes of cluster 7 along the pseudotime. **(K)** Bubble plot showing enrichment of GO biological processes using cluster 7 DEGs

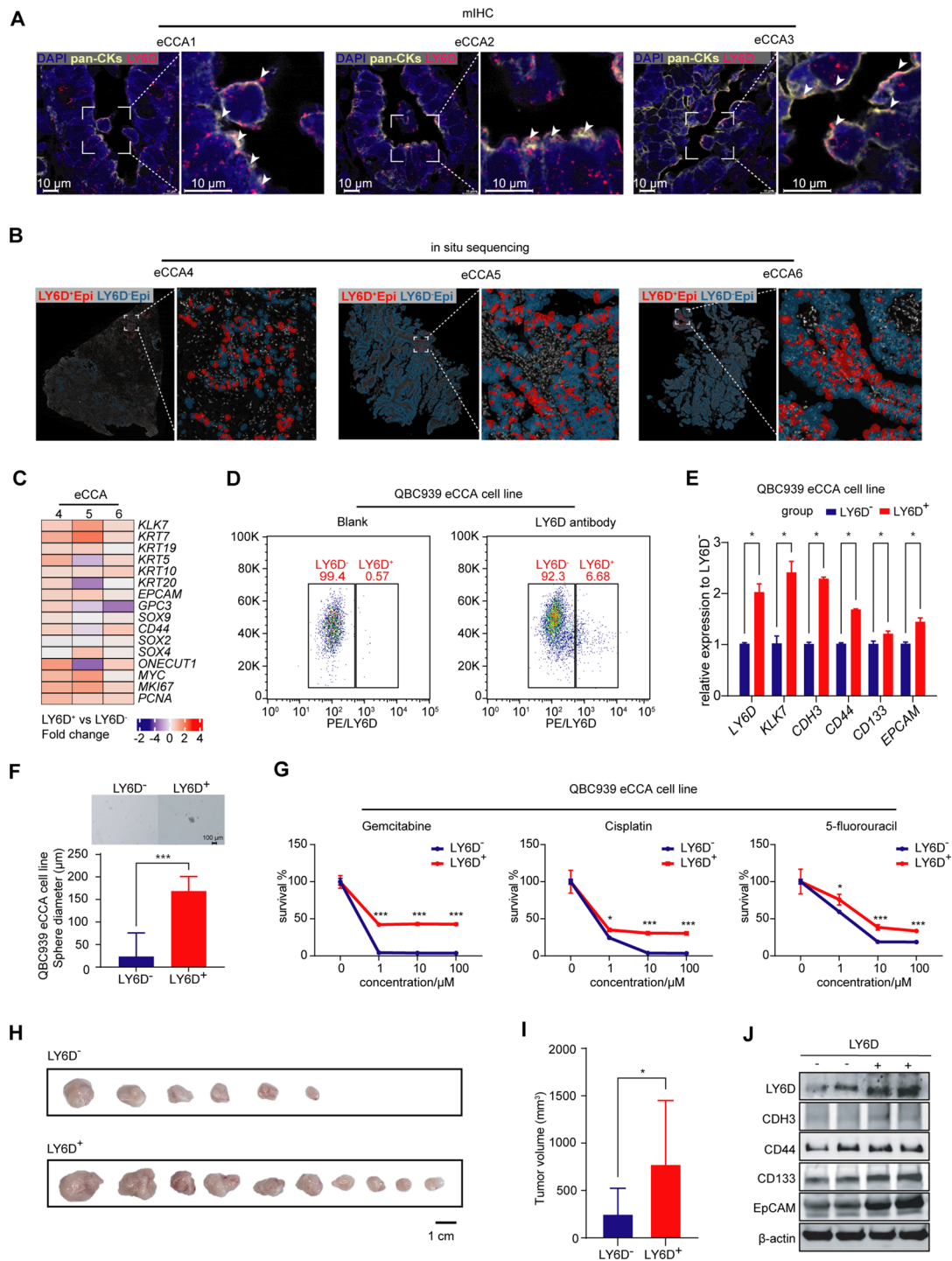


**Fig. 5** eCCA-specific basal-like progenitors showing basal cell and stemness features, with increased drug resistance. **(A)** Multiplex IHC of LY6D<sup>+</sup> EPCs in three eCCA patients, indicated by white arrows. DAPI: deep blue. Pan-CK: light yellow. LY6D: pink. Scale bar: 10  $\mu$ m. **(B)** RNA in situ sequencing of three eCCA patients. LY6D<sup>+</sup> and LY6D<sup>-</sup> EPCs are labeled by red and blue, respectively. Cell nuclei are labeled by white. **(C)** RNA in situ sequencing revealing differential expression of basal, stemness and proliferative marker genes between LY6D<sup>+</sup> and LY6D<sup>-</sup> EPCs. **(D)** Sorting of LY6D<sup>+</sup> and LY6D<sup>-</sup> subpopulations in QBC-939 eCCA cell line by flow cytometry. **(E)** Bar plot comparing RT-qPCR results of marker genes between LY6D<sup>+</sup> and LY6D<sup>-</sup> subpopulations of the QBC-939 eCCA cell line. **(F)** Barplot comparing spheroid formation capacity between LY6D<sup>+</sup> and LY6D<sup>-</sup> subpopulations of the QBC-939 eCCA cell line. **(G)** Dose-response curves showing differential responses to gemcitabine, cisplatin, and 5-fluorouracil between LY6D<sup>+</sup> and LY6D<sup>-</sup> subpopulations of QBC-939 eCCA cell line. **(H)** Photos comparing subcutaneous tumor growth after injection of LY6D<sup>+</sup> and LY6D<sup>-</sup> populations from the QBC-939 eCCA cell line in nude mice. **(I)** Bar plot comparing average tumor volumes after injecting LY6D<sup>+</sup> or LY6D<sup>-</sup> cells. **(J)** Western blot analyses comparing protein expression of LY6D and stemness markers between LY6D<sup>+</sup> and LY6D<sup>-</sup> tumors. Statistical analyses are from t-test. \*,  $p < 0.05$ ; \*\*,  $p < 0.01$ ; \*\*\*,  $p < 0.001$

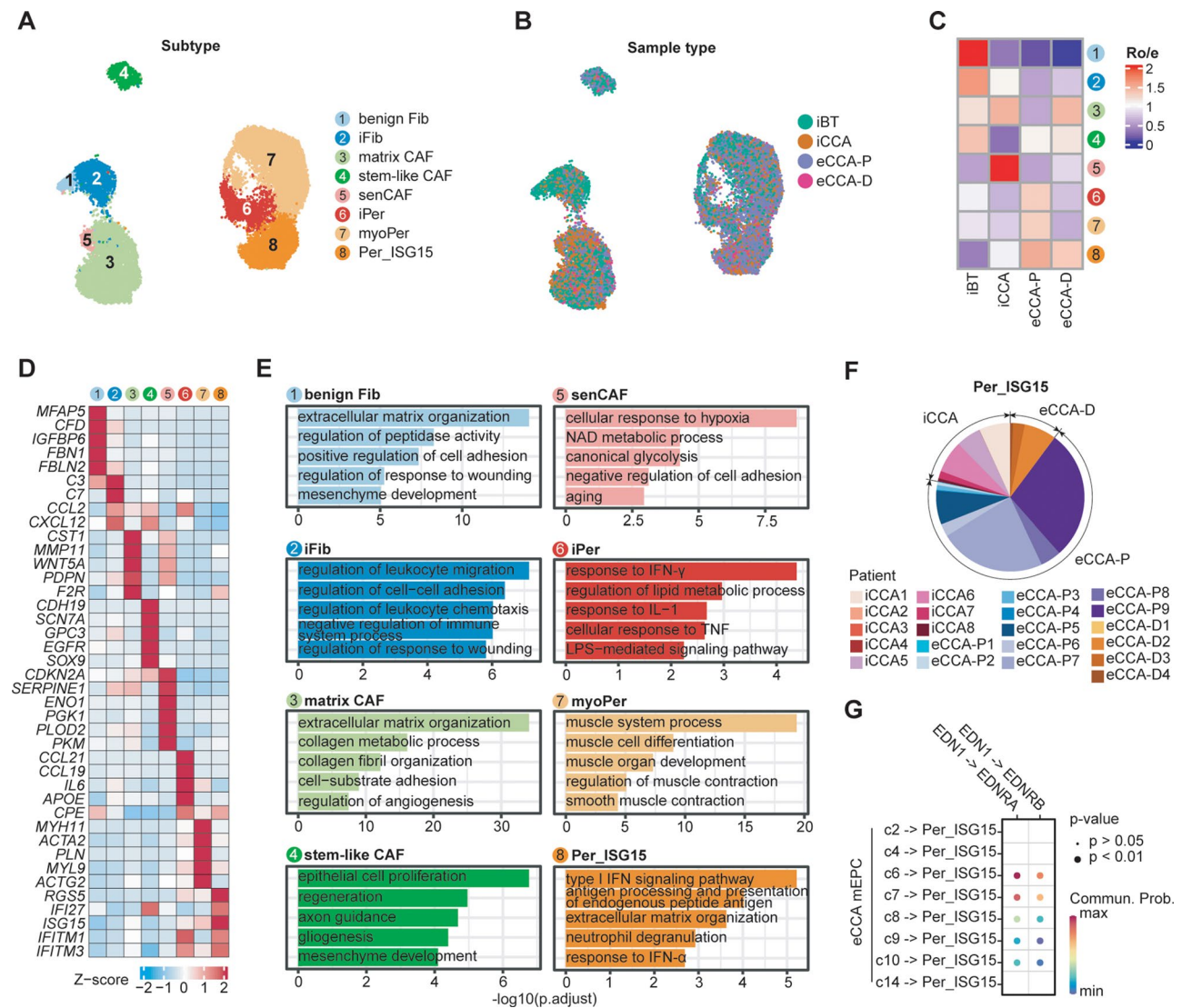


**Fig. 6** scRNA-seq analysis of CCA mesenchymal microenvironment. **(A)** UMAP showing the mesenchymal cells colored by cell subtypes. iFib, inflammatory fibroblast; senCAF, senescent CAF; iPer, inflammatory pericyte; myoPer, myofibroblast pericyte. **(B)** UMAP showing mesenchymal cells colored by sample types. **(C)** Sample preference of the mesenchymal subtypes analyzed by Ro/e. **(D)** Heatmap showing average expression of marker genes across eight mesenchymal subtypes. **(E)** Barplots showing enrichment of GO biological processes across eight mesenchymal subtypes. **(F)** Pie chart displaying the percentage contribution of sample sources in ISG15 Per. **(G)** Bubble plot showing cell-cell interaction of EDN signaling pathways between eCCA mEPC subclusters and Per\_ISG15

Uniquely expressing pro-inflammatory markers (*CCL19*, *CCL21*, *IL6*), c6 was defined as inflammatory pericytes (iPer). Myopericytes (myoPer, c7) highly expressed *MYH11* and *ACTA2*, associated with smooth muscle contraction. Both iPer and myoPer clusters were enriched in eCCA-Ps. We also identified a subset of pericytes (c8; Per\_ISG15 highly expressing interferon-stimulated genes (ISGs) such as *ISG15*, *IFI27*, and *IFITM1/3*, predominantly enriched in eCCA-Ps and eCCA-Ds (Figs. 6B-F). ISGs like *ISG15* operate both intracellularly and extracellularly, acting as central players in IFN-associated pathways and vividly modulating the host damage and repair response [27]. Cell-cell communication

analyses revealed robust interaction between Per\_ISG15 and c7 mEPC cluster, primarily mediated by EDN1 and EDNRA/B ligand-receptor interaction (Fig. 6G).

#### Immune landscape of CCAs revealing eCCA-specific *ISG15*<sup>high</sup> subsets

Immune cell profiles (e.g., macrophages, T cells) surrounding bile ducts likely establish site-specific immune compartmentalization that dictate localized immune surveillance, yet remain largely uncharted [28]. We firstly identified two monocyte clusters (*S100A8*<sup>+</sup>*S100A9*<sup>+</sup>), seven macrophage clusters (*CD68*<sup>+</sup>*CD163*<sup>+</sup>), and four dendritic cell clusters (*FCERIA*<sup>+</sup>*HLA-DQA1*<sup>+</sup>) (Figs. 7A,

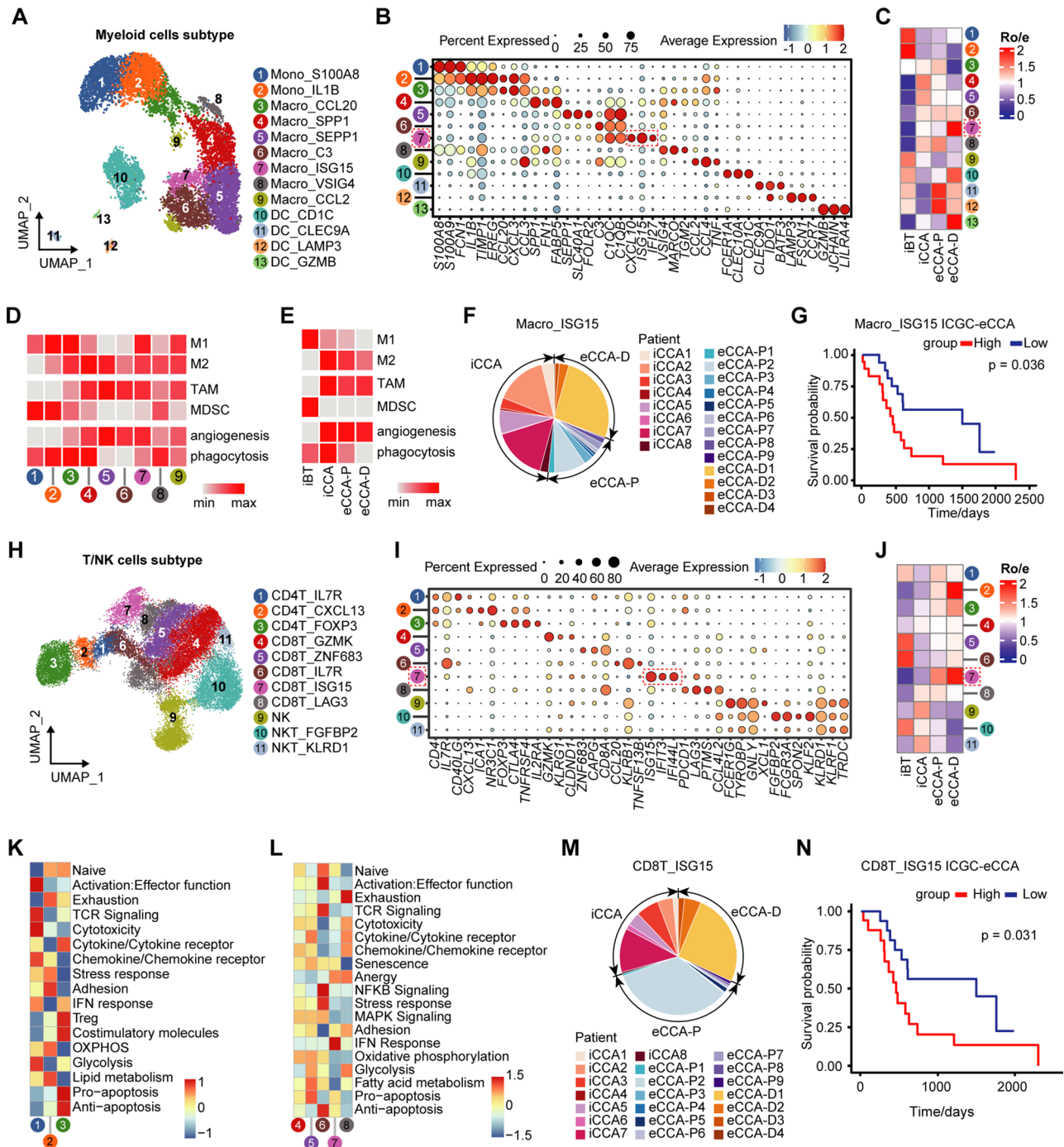


**Fig. 7** scRNA-seq revealing IFN-signaling activated immune subpopulations. **(A)** UMAP of myeloid cells colored by subtypes. Mono, monocytes; Macro, macrophages; DC, dendritic cells. **(B)** Bubble plots showing the expression of marker genes across myeloid cell subtypes. **(C)** Sample preference of myeloid cells subtypes analyzed by Ro/e. **(D)** Heatmap showing functional enrichment scores across monocyte and macrophage subtypes. TAM, tumor-associated macrophage. **(E)** Heatmap showing functional enrichment scores across different sample types. **(F)** Pie chart displaying the percentage contribution of sample sources in Macro\_ISG15. **(G)** Kaplan-Meier curves of overall survival in ICGC-eCCA cohort patients grouped by Macro\_ISG15 signature score. **(H)** UMAP visualization of lymphocytes colored by subtypes. **(I)** Bubble plot showing the expression of marker genes of lymphocyte subtypes. **(J)** Sample preference of lymphocyte subtypes analyzed by Ro/e. **(K, L)** Heatmap showing functional enrichment scores of CD4<sup>+</sup> T cell and CD8<sup>+</sup> T cell subtypes. **(M)** Pie chart displaying the percentage contribution of sample sources in CD8T\_ISG15. **(N)** Kaplan-Meier curves of overall survival in ICGC-eCCA cohort patients grouped by CD8T\_ISG15 signature score

B and S10A; Table S8) with differential distributions and functional phenotypes (Figs. 7C-E). Akin to our findings in gallbladder cancer [29], we observed an enrichment of myeloid-derived suppressor cell (MDSC)-like monocytes in iBTs. M2-like macrophages and tumor-associated macrophages (TAMs) were more prevalent in CCAs. The Macro\_ISG15 cluster highly expressed ISGs (e.g., *ISG15*, *IFI27*) and was preferentially enriched in eCCAs (Figs. 7C and F). Deconvolution of the ICGC microarray dataset using Macro\_ISG15 signatures showed that higher expression correlated with shortened survival in eCCAs but not in iCCAs (Figs. 7G and S10C). Cell-cell communication analysis revealed active interaction between the c7 mEPC cluster and Macro\_ISG15 via the GAS6-AXL signaling pathway (Fig. S10B).

We further characterized three CD4<sup>+</sup> T cell clusters, five CD8<sup>+</sup> T cell clusters, two NKT clusters, and one NK cluster (Figs. 7H and S10D). We annotated the CD4T\_IL7R cluster as cytotoxic effector CD4<sup>+</sup> T cells, the CD4T\_CXCL13 cluster as exhausted T cells, and the CD4T\_FOXP3 cluster as regulatory T cells (Fig. 7K). Similarly, we characterized naïve T cells (CD8T\_IL7R), cytotoxic T cells (CD8T\_GZMK), exhausted T cells (CD8T\_LAG3), and tissue-resident memory T cells (CD8T\_ZNF683) (Fig. 7L). Notably, we identified a sub-cluster of CD8<sup>+</sup> cells (CD8T\_ISG15) highly expressing *ISG15*, *IFIT3* and *IFI44L* (Fig. 7I), enriched in eCCAs (Figs. 7J and M), and showed enrichment of IFN response pathways (Fig. 7L). Deconvolution of the ICGC dataset revealed that elevated expression of CD8T\_ISG15 signatures portended worse prognosis for eCCAs but not for iCCAs (Figs. 7N and S10E).

#### Validation of specific mesenchymal and immune niches for basal-like progenitors

The data presented above revealed a convergence of specific epithelial, mesenchymal, and immune cell subpopulations (Clusters of mEPC\_c7, Per\_ISG15, Macro\_ISG15, and CD8T\_ISG15) surrounding eCCAs (Fig. 8A), which prompted a deeper exploration of their interconnected associations. All of these clusters consistently exhibited elevated expression of multiple ISGs, particularly ISG15 (Fig. 8B), in line with the notion that ISG15 is one of the most rapidly and strongly induced ISGs [27]. Analysis of the public ICGC dataset confirmed higher expression of ISG15 in eCCAs compared to iCCAs (Fig. 8C). In eCCA patients, ISG15 expression correlated strongly with *LY6D*<sup>+</sup> mEPC signatures (e.g., *LY6D*, *KLK7*, *KRT5*, *CDH3*) and was associated with worse prognosis (Figs. 8D-E). By examining the aforementioned external single-cell datasets of eCCAs, we validated the presence of *ISG15*<sup>high</sup> cell clusters across pericytes, myeloid cells, and T/NK cells (Figs. S11A-I). Leveraging annotated markers of major cell types from scRNA-seq, we identified spatial

co-location patterns between *LY6D*<sup>+</sup> EPCs and *ISG15*<sup>high</sup> pericytes, *ISG15*<sup>high</sup> CD8<sup>+</sup> T cells, and *ISG15*<sup>high</sup> macrophages in RNA ISS experiments (Figs. 8F and S12A). Among the three *ISG15*<sup>high</sup> TME subsets, Per\_ISG15 cells were found to reside in significantly closer proximity to *LY6D*<sup>+</sup> EPCs, suggesting a preferential spatial relationship (Fig. S12B).

Given the progenitor-like property of *LY6D*<sup>+</sup>*KLK7*<sup>+</sup> mEPCs, we hypothesized that ISG15 might play a role in sustaining this feature. Using the tumor spheroid assay with the eCCA-P cell line QBC-939, we confirmed that ISG15 stimulation significantly increased the spheroid formation capacity of cancer cells (Figs. 8G, H). Quantitative real-time PCR and western blotting (WB) validated the upregulation of basal cell markers (*LY6D*, *KLK7*) and stem cell markers (*CD44*, *CD133*, *EPCAM*) (Figs. 8I, J). To further elucidate the role of ISG15 in functional precision oncology, we introduced ISG15 into eCCA PDO and cell line models, and evaluated the vulnerability of cisplatin, gemcitabine, and 5-FU. ISG15 markedly enhanced resistance of cisplatin and gemcitabine in the PDO line, and to cisplatin and 5-FU in the cell line (Fig. S13A). Moreover, using an IFN-responsive PDO line, we proved that the addition of ISG15 could substantially increase resistance to most tested compounds, including those targeting DNA damage, epigenetic reprogramming, or cytoskeletal signaling (Fig. S13B), reminiscent of the drug-resistant features of IFN-responsive PDOs (Fig. 3C).

Collectively, we identified a subpopulation of *LY6D*<sup>+</sup> basal-like progenitors uniquely localized within eCCAs, likely sustained by *ISG15*<sup>high</sup> mesenchymal and immune niches. ISG15 is crucial for maintaining cancer cell stemness and augmenting resistance to various anti-cancer agents.

#### Discussion

Despite the rapid expansion of single-cell studies, data on CCAs, particularly eCCAs, remains scarce, impeding our understanding of therapeutic or prognostic discrepancies between CCA subgroups in clinical trials [30]. We endeavored to address this gap by presenting a single-cell atlas of different CCA subtypes and predisposing inflammatory conditions. Consistent with our prior findings in chronic cholecystitis [29], we identified gastrointestinal metaplastic cell states in cholangiocytes within inflammatory EBTs, suggesting a conservative mechanism of hijacking reparative programs in response to mucosal injury or inflammation across the extrahepatic biliary system. In contrast, benign EPCs (*CNV*<sup>low</sup>) within tumors exhibited more pronounced activation of onco-fetal, EMP, and immune-regulating programs, which were preferentially enriched within iCCAs, eCCA-Ps, and eCCA-Ds, respectively. These findings enhanced our

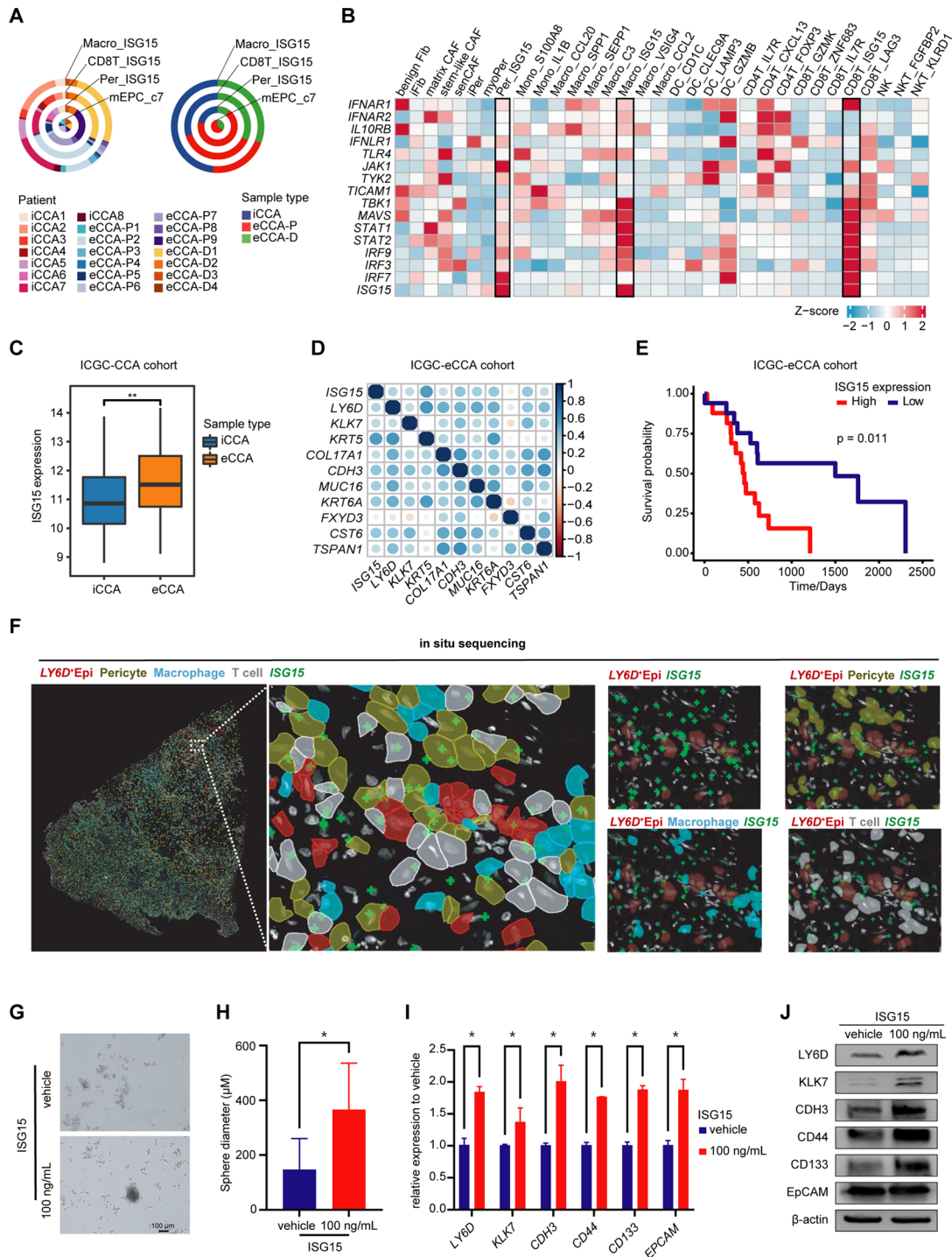


**Fig. 8** Specific mesenchymal and immune niches sustaining basal-like progenitors. **(A)** Circular plot displaying the distribution of sample sources for Macro\_ISG15, CD8T\_ISG15, Per\_ISG15 and mEPC\_c7: patient sources (left) and sample type origins (right). **(B)** Heatmap showing average expression of *ISG15* and representative upstream genes across mesenchymal and immune cell subtypes. **(C)** Boxplot comparing *ISG15* expression levels between iCCAs and eCCAs in the ICGC cohort. **(D)** Correlation heatmap analyzing expression of *ISG15* and representative DEGs of c7 mEPC clusters in ICGC eCCA patients. **(E)** Kaplan-Meier curves of overall survival in eCCA patients stratified by *ISG15* expression in the ICGC-eCCA dataset. **(F)** Spatial RNA ISS visualization of *LY6D*<sup>+</sup> EPCs and *ISG15*-expressing pericytes, macrophages and T cells. *LY6D*<sup>+</sup> EPCs: red. Pericytes: light brown, Macrophages: light blue. T cells: grey. *ISG15*: green cross. **(G, H)** Spheroid formation capacity analysis between vehicle- and *ISG15* (100 ng/mL)-treated QBC-939 eCCA cell line. **(I)** Bar plot comparing RT-qPCR results of marker genes between vehicle- and *ISG15* (100 ng/mL)-treated QBC-939 eCCA cell line. **(J)** WB analysis comparing proteins levels of *LY6D*, *KLK7* and stemness markers between vehicle- and *ISG15* (100 ng/mL)-treated QBC-939 eCCA cell line. Statistical analyses are obtained from t-test. \*,  $p < 0.05$ ; \*\*,  $p < 0.01$ ; \*\*\*,  $p < 0.001$

understanding of biliary-associated and site-specific precancer hallmarks [6].

Moreover, iCCAs and eCCAs displayed substantial differences in terms of cellular composition, diversity, and abundance of various cell types, which likely reflected their distinct embryonic origins, histological structures, and patterns of cellular crosstalk [31]. Unlike eCCAs, iCCAs exhibit a broader range of cell lineages and genetic alterations [32]. For instance, iCCAs share genetic overlap with eCCAs on one end (78%) and with hepatocellular carcinomas (HCCs) on the other (23%) [33]. Specific genomic alterations, such as *FGFR2* and *IDH1*, are uniquely found in iCCAs (~20%) but absent in eCCAs (0%) [34]. Accordingly, we showed that iCCAs displayed greater inter-tumoral heterogeneity compared to eCCAs.

To gain a deeper understanding of the CCA heterogeneity, we identified both convergent and divergent transcriptomic signatures within cancer cells from iCCAs and eCCAs, which were mapped to four molecular subtypes: proliferative, senescent, glandular, and IFN-responsive. Importantly, the molecular subtyping was recapitulated in PDO models and validated across multiple independent multi-omics datasets, offering valuable tools for pharmacotyping and prognostic prediction. iCCAs exhibited a uniquely activated senescent programs with associated SASP, evident in both cholangiocytes and surrounding fibroblasts. Cholangiocyte senescence is closely linked to hepatic ductular reaction, commonly observed in response to inflammation or fibrosis around the canals of Hering [35]. Senescent fibroblasts were featured by active glycolytic metabolic and senescent reprogramming, reminiscent of a subpopulation of senescent HSCs [26]. These cells were always marked by heightened DNA repair and reactive oxygen species (ROS) activities secondary to senescence-induced DNA damage [36]. The SASP milieu likely contributed to a “tissue inflammaging” immunosuppressive TME, thus driving tumor initiation, progression, and therapeutic resistance [10, 37].

Intriguingly, we uncovered a cluster of *LY6D*<sup>+</sup> basal-like malignant cells predominantly enriched in eCCA samples. The basal-like program is a hallmark of tumors arising from stratified squamous epithelium [38]. However, this program has also been observed in tumors arising from glandular columnar epithelia across lung, breast, prostate, or pancreas [39–43]. Our basal-like subpopulation exhibited greater stemness and drug resistance, typically behaving as progenitor cells and drug-tolerant persister cells [44]. Similarly, basaloid features in other cancer subtypes are associated with poor differentiation, heightened drug resistance, and unfavorable prognosis [41–43]. Notably, the initial default specification of the entire gut tube is the anterior foregut endoderm during development, mostly typified by the esophageal basal cell

features [45]. The hepatobiliary system shares the foregut developmental path with the esophagus, and thus cholangiocytes may assume a basal-like state by traversing the developmental map through early foregut progenitor states [15, 46].

The exceedingly rarity of squamous tumors across the biliary tree also implied a multipotent plasticity rather than squamous-committed fate of *LY6D*<sup>+</sup> progenitor cells [47]. Classical non-melanoma skin cancers are dichotomized into basal and squamous subtypes, with the former displaying increased stemness. In esophagus, deeper basal cells (*KRT5*<sup>+</sup>*KRT14*<sup>+</sup>*CDH3*<sup>+</sup>) display increased stemness capacity compared to the above suprabasal cells (*KRT4*<sup>+</sup>*KRT13*<sup>+</sup>) [48]. Notably, our basal-like cholangiocyte cluster (*KRT5*<sup>+</sup>*KRT14*<sup>+</sup>*CDH3*<sup>+</sup>) was more like deeper progenitor basal cells in skin or esophagus [15]. Upon revisiting several literature claiming adeno-squamous transformation under therapeutic pressure [49, 50], we found that the claimed “squamous” cells aligned more closely with basal progenitors rather than differentiated squamous cells.

The eCCA-specific *LY6D*<sup>+</sup> basal-like progenitors exhibited significantly elevated IFN response scores and activation of IFN signaling pathways. Several *ISG15*<sup>high</sup> TME components, including pericytes, macrophages, and CD8<sup>+</sup> T cells, were consistently enriched within eCCAs and spatially located in proximity to *LY6D*<sup>+</sup> mEPCs, which engaged in vivid cellular crosstalk with these progenitor cells and sustained their stemness. For example, Macro\_IGS15 likely interacted with c7 mEPC cluster via the GAS/TAM signaling axis, which promoted the emergence of *ISG15*<sup>high</sup> macrophage by activating the downstream JAK/STAT3/ISG15 signaling cascade [51]. Similarly, mEPCs presumably induced chemotaxis of Per\_IGS15 via the EDN1-EDNRA/B signaling pathway, which fostered a specialized perivascular niche [52], reminiscent of previous evidence that pericytes help maintain a stem cell niche in bone marrow and fetal liver [53]. Prior studies have suggested the existence of non-fetal stem cell niches in adult tissues, such as hepatocytes and cholangiocytes within the canals of Hering, as well as hepatocytes, cholangiocytes, and insulin-secreting cells from the peribiliary glands [54]. Our findings offer novel evidence for the presence of basal-like progenitor cell niches within the extrahepatic biliary tree and expand the understanding of stem cell plasticity in bile ducts.

Integrated TME analyses narrowed our focus on the role of ISG15 and associated type I IFN pathways in maintaining the *LY6D*<sup>+</sup> basal-like progenitors [27]. External multi-omics datasets and experimental validation confirmed that ISG15 signaling is critical for sustaining the basal-like stemness of mEPCs. The intrinsic expression of ISGs is a conserved feature across mammalian stem cells [55]. For instance, The IFN signaling protects

intestinal crypt base cells from differentiation, thereby preserving their stemness [56]. Similarly, type I IFN has been shown to enhance breast cancer cell stemness and promote drug resistance [57]. Importantly, considering the central role of chronic activation of type I IFN signaling in driving “trained immunity” and facilitating immune evasion in cancers [58], ISG15 presumably serves as a ‘master coach’, training cancer cells the art of survival.

Moreover, ISG15 signaling appeared to be more actively engaged in eCCAs compared to iCCAs. Under physiological conditions, low-level type I IFN signaling helps maintain liver homeostasis and sustains immune tolerance [59, 60]. However, hyperactivated type I IFN signaling in the liver could lead to autoimmune liver diseases [61]. In comparison to liver-resident small cholangiocytes, large cholangiocytes exhibit stronger regenerative, proliferative, and apoptotic responses to injury or toxic insults [62–64]. These cellular activities likely drive the accumulation of extrachromosomal DNAs, which may elicit robust cGAS-STING signaling and amplify type I IFN signaling in EBTs [65, 66]. Moreover, microbiota dysbiosis caused by malignant biliary obstruction [67], as well as direct contact with bile flow and bile acids [68, 69], may further heighten the activation of ISG15-associated type I IFN signaling within eCCAs [70].

Several limitations of this study warrant consideration. First, our cohort may not capture the full diversity of CCAs, particularly the primary sclerosing cholangitis (PSC)-associated cases prevalent in Western populations [71]. Second, we mainly annotated cell types based on established marker genes, which may limit the detection of previously uncharacterized or rare cell populations or states. While we identified key ISG15<sup>high</sup> cell types within the TME, further investigation is required to explore other immune subsets, such as B cells, NK cells, and mast cells. Moreover, considering the pivotal role of the PD-1/CTLA-4 axis in BTCs [72], integrating ISG15-associated pathways into the current immunotherapy framework remains an unexplored area. Although PDOs are valuable for personalized drug testing, they do not fully recapitulate the complexity of TME. The absence of immune and stromal components in PDOs may limit the interpretation of our drug resistance data. More sophisticated co-culture PDO systems hold promise for more accurately assessing drug efficacy and understanding how the ISG15<sup>high</sup> TME influences cancer cell behavior in vivo. We also recognized the growing evidence regarding the dual roles of IFN response pathways in cancer [65]. To elucidate the multifaceted functions of ISG15 in BTCs, particularly its involvement in DNA damage repair, type I IFN-mediated immune evasion, and intracellular ISGylation processes [27, 73, 74], additional functional

experiments, including genetic knockout mouse models, will be needed. Lastly, the clinical applicability of biomarkers such as LY6D and ISG15 remains to be fully validated by larger clinical cohort and multi-omics dataset. Further clinical research will be essential to translation our findings into clinic.

## Conclusions

Our study presents a comprehensive single-cell atlas that delineates the transcriptomic diversity, heterogeneity, and phenotypic subtyping of CCAs, broadening our understanding of the biliary ecosystem [75]. We uncover a spectrum of cancer cell states associated with CCA subtyping, drug vulnerability, and prognosis. Notably, iCCAs and eCCAs are distinguished by senescent and IFN-responsive programs, respectively, which are sustained by unique senescent or IFN-activated TMEs. For the first time, we identified a LY6D<sup>+</sup> basal-like progenitor subpopulation unique for eCCAs, which is nurtured by ISG15-enriched TME niches. ISG15 signaling within the TME facilitates the emergence and maintenance of these progenitor cells, and contribute to drug resistance. The identification of basal-like progenitor cells and associated ISG15-enriched TME in eCCAs potentially opens new avenues for the development of prognostic biomarkers and precision oncology regimens targeting the progenitor cell niches.

## Abbreviations

CAF	Cancer-associated fibroblast
CCA	Cholangiocarcinoma
EBT	Extrahepatic bile duct
eCCA	Extrahepatic cholangiocarcinoma
eCCA-D	Distal cholangiocarcinoma
eCCA-P	Perihilar cholangiocarcinoma
EPCs	Epithelial cells
HSC	Hepatic stellate cell
iCCA	Intrahepatic cholangiocarcinoma
ICGC	International Cancer Genome Consortium
IFN	Interferon
iPer	Inflammatory pericyte
ISG15	Interferon-stimulated gene 15
ISS	In situ sequencing
MDSC	Myeloid-derived suppressor cell
mIHC	Multicolor immunohistochemical
MPs	Meta-programs
NF	Normal fibroblast
NMF	Non-negative matrix factorization
PDO	Patient-derived organoid
scRNA-seq	Single-cell RNA sequencing
TAM	Tumor-associated macrophage
TME	Tumor microenvironment

## Supplementary Information

The online version contains supplementary material available at <https://doi.org/10.1186/s13045-025-01716-z>.

Supplementary Material 1

Supplementary Material 2

Supplementary Material 3

Supplementary Material 4  
Supplementary Material 5  
Supplementary Material 6  
Supplementary Material 7  
Supplementary Material 8  
Supplementary Material 9  
Supplementary Material 10  
Supplementary Material 11  
Supplementary Material 12  
Supplementary Material 13  
Supplementary Material 14  
Supplementary Material 15  
Supplementary Material 16  
Supplementary Material 17  
Supplementary Material 18  
Supplementary Material 19  
Supplementary Material 20  
Supplementary Material 21  
Supplementary Material 22

### Acknowledgements

We thank patients and doctors in Eastern Hepatobiliary Hospital for help with the collection of clinical samples. We would like to express our sincere gratitude to Drs. Wei Yao and Lei Xu at the Tongji Medical College, Huazhong University of Science and Technology, for generously providing the scRNA-seq data of eCCAs (PMID: 35562760). We also thank Prof. Xiaolu Zhang at the School of Basic Medical Sciences, Cheeloo College of Medicine, Shandong University, for sharing the scRNA-seq data of eCCAs (PMID: 35219893).

### Author contributions

JF, HYW and JT contributed to the study conceptualization, design, and supervision. XW, WLY, and YL contributed to sample acquisition, collection of clinical information, and patients' follow-up. CLL, XW, JAC, MYG, ZYM, JFL, YJZ, and JF made contributions to collection, analyses, and interpretation of the data. CLL, XW, EDL, and JAC were responsible for the visualization of the data. JF, HYW, XW and CLL were involved in funding support. XW, CLL, EDL, JAC, and JF contributed to writing the draft. JF, HYW, CLL, XW, EDL, and JAC revised the manuscript. All authors reviewed, discussed, and approved the final manuscript.

### Funding

This study is supported by the National Research Program of China (2022YFC3400902), the National Natural Science Foundation of China (82588201, 82472807, 82425038, 82421005, 82203209, 82172977), Shanghai Discipline Leaders Program (2022XD058), China Postdoctoral Science Foundation (2022M720786), the Shanghai "Rising Stars of Medical Talents" Youth Development Program-Youth Medical Talents-Specialist Program (SHWSRS (2024)\_070), Basic Medical Research Youth Program of Naval Medical University (2022QN042), and the Natural Science Foundation of Shanghai (25JS2850300).

### Data availability

The raw FASTQ files of our single-cell RNA sequencing of CCA patients are available from the Genome Sequence Archive for Human (GSA-Human) at the China National Center for Bioinformatics (CNCB) (accession code HRA010272). All other data supporting the results of this study are available from the corresponding author on reasonable request.

### Declarations

#### Ethics approval and consent to participate

This study was approved by the Ethical Committee of Eastern Hepatobiliary Surgery Hospital (No. EHBHKY2018-1-001). Written informed consent was obtained from each patient involved in the CCA scRNA-seq cohort.

#### Competing interests

The authors declare no competing interests.

#### Author details

- <sup>1</sup>International Cooperation Laboratory on Signal Transduction, National Center for Liver Cancer, Ministry of Education Key Laboratory on Signaling Regulation and Targeting Therapy of Liver Cancer, Shanghai Key Laboratory of Hepato-Biliary Tumor Biology, Eastern Hepatobiliary Surgery Hospital, Naval Medical University, Shanghai 200438, China  
<sup>2</sup>Second Department of Biliary Surgery, Eastern Hepatobiliary Surgery Hospital, Naval Medical University, Shanghai 200438, China  
<sup>3</sup>Institute of Metabolism & Integrative Biology, Fudan University, Shanghai 200433, China  
<sup>4</sup>Cancer Research Center, Division of Life Sciences and Medicine, The First Affiliated Hospital of USTC, University of Science and Technology of China, Hefei, Anhui 230001, China  
<sup>5</sup>State Key Laboratory of Oncogenes and Related Genes, Renji Hospital, Shanghai Cancer Institute, Shanghai Jiao Tong University School of Medicine, Shanghai 200127, China  
<sup>6</sup>Cancer Center, Union Hospital, Tongji Medical College, Huazhong University of Science and Technology, Wuhan 430022, China  
<sup>7</sup>1277 Jiefang Avenue, Shanghai, Hubei 200438, China

Received: 7 October 2024 / Accepted: 31 May 2025

Published online: 23 June 2025

### References

1. Rushbrook SM, Kendall TJ, Zen Y, Albazaz R, Manoharan P, Pereira SP, et al. British society of gastroenterology guidelines for the diagnosis and management of cholangiocarcinoma. *Gut*. 2023;73(1):16–46.
2. Qurashi M, Vithayathil M, Khan SA. Epidemiology of cholangiocarcinoma. *Eur J Surg Oncol* 2023;107064.
3. Jusakul A, Cutcutache I, Yong CH, Lim JQ, Huang MN, Padmanabhan N, et al. Whole-genome and epigenomic landscapes of etiologically distinct subtypes of cholangiocarcinoma. *Cancer Discov*. 2017;7(10):1116–35.
4. Strazzabosco M, Fabris L. Development of the bile ducts: essentials for the clinical hepatologist. *J Hepatol*. 2012;56(5):1159–70.
5. Lanzoni G, Cardinale V, Carpino G. The hepatic, biliary, and pancreatic network of stem/progenitor cell niches in humans: A new reference frame for disease and regeneration. *Hepatology*. 2016;64(1):277–86.
6. Stangis MM, Chen Z, Min J, Glass SE, Jackson JO, Radyk MD, et al. The hallmarks of precancer. *Cancer Discov*. 2024;14(4):683–9.
7. Hodgall D, Lewinska M, Andersen JB. Desmoplastic tumor microenvironment and immunotherapy in cholangiocarcinoma. *Trends Cancer*. 2018;4(3):239–55.
8. Scott AJ, Sharman R, Shroff RT. Precision medicine in biliary tract cancer. *J Clin Oncol*. 2022;40(24):2716–34.
9. Chen LT, Vogel A, Hsu C, Chen MH, Fang W, Pangarsa EA, et al. Pan-Asian adapted ESMO clinical practice guidelines for the diagnosis, treatment and follow-up of patients with biliary tract cancer. *ESMO Open*. 2024;9(8):103647.
10. Suryadevara V, Hudgins AD, Rajesh A, Pappalardo A, Karpova A, Dey AK, et al. SenNet recommendations for detecting senescent cells in different tissues. *Nat Rev Mol Cell Biol*. 2024;25(12):1001–23.
11. van Renterghem AWJ, van de Haar J, Voest EE. Functional precision oncology using patient-derived assays: bridging genotype and phenotype. *Nat Rev Clin Oncol*. 2023;20(5):305–17.
12. Jiang S, Zhao H, Zhang W, Wang J, Liu Y, Cao Y, et al. An automated organoid platform with inter-organoid homogeneity and inter-patient heterogeneity. *Cell Rep Med*. 2020;1(9):100161.
13. Vincent F, Nueda A, Lee J, Schenone M, Prunotto M, Mercola M. Phenotypic drug discovery: recent successes, lessons learned and new directions. *Nat Rev Drug Discov*. 2022;21(12):899–914.

14. Vieira AF, Ricardo S, Ablett MP, Dionisio MR, Mendes N, Albergaria A, et al. P-cadherin is coexpressed with CD44 and CD49f and mediates stem cell properties in basal-like breast cancer. *Stem Cells*. 2012;30(5):854–64.
15. Moon H, Zhu J, Donahue LR, Choi E, White AC. Krt5(+)/Krt15(+) foregut basal progenitors give rise to cyclooxygenase-2-dependent tumours in response to gastric acid stress. *Nat Commun*. 2019;10(1):2225.
16. Inlay MA, Bhattacharya D, Sahoo D, Serwold T, Seita J, Karsunky H, et al. Ly6d marks the earliest stage of B-cell specification and identifies the branchpoint between B-cell and T-cell development. *Genes Dev*. 2009;23(20):2376–81.
17. Xu L, Lu Y, Deng Z, Li X, Shi Y, Zhao K, et al. Single-cell landscape of immunocytes in patients with extrahepatic cholangiocarcinoma. *J Transl Med*. 2022;20(1):210.
18. Li H, Qu L, Yang Y, Zhang H, Li X, Zhang X. Single-cell transcriptomic architecture unraveling the complexity of tumor heterogeneity in distal cholangiocarcinoma. *Cell Mol Gastroenterol Hepatol*. 2022;13(5):1592–e16091599.
19. Heij L, Hayat S, Reichel K, Maryam S, O'Rourke CJ, Tan X et al. Shift in cellular crosstalk reveals the immunosuppressive environment in cholangiocarcinoma patients. *bioRxiv* 2024:2024.2002.2003.578669.
20. Affo S, Nair A, Brundu F, Ravichandra A, Bhattacharjee S, Matsuda M, et al. Promotion of cholangiocarcinoma growth by diverse cancer-associated fibroblast subpopulations. *Cancer Cell*. 2021;39(6):866–e882811.
21. van Splunder H, Villacampa P, Martinez-Romero A, Graupera M. Pericytes in the disease spotlight. *Trends Cell Biol*. 2024;34(1):58–71.
22. Olijnyk D, Ibrahim AM, Ferrier RK, Tsuda T, Chu ML, Gusterson BA, et al. Fibulin-2 is involved in early extracellular matrix development of the outgrowing mouse mammary epithelium. *Cell Mol Life Sci*. 2014;71(19):3811–28.
23. Vaitinen M, Kolehmainen M, Ryden M, Eskelinen M, Wabitsch M, Pihlajamaki J, et al. MFAP5 is related to obesity-associated adipose tissue and extracellular matrix remodeling and inflammation. *Obes (Silver Spring)*. 2015;23(7):1371–8.
24. Fonovic M, Turk B. Cysteine cathepsins and extracellular matrix degradation. *Biochim Biophys Acta*. 2014;1840(8):2560–70.
25. Suryadevara V, Hudgins AD, Rajesh A, Pappalardo A, Karpova A, Dey AK et al. SenNet recommendations for detecting senescent cells in different tissues. *Nat Rev Mol Cell Biol* 2024.
26. Trivedi P, Wang S, Friedman SL. The power of plasticity-metabolic regulation of hepatic stellate cells. *Cell Metab*. 2021;33(2):242–57.
27. Perng YC, Lenschow DJ. ISG15 in antiviral immunity and beyond. *Nat Rev Microbiol*. 2018;16(7):423–39.
28. Bjorkstrom NK. Immunobiology of the biliary tract system. *J Hepatol*. 2022;77(6):1657–69.
29. Wang X, Liu C, Chen J, Chen L, Ren X, Hou M, et al. Single-cell dissection of remodeled inflammatory ecosystem in primary and metastatic gallbladder carcinoma. *Cell Discov*. 2022;8(1):101.
30. McNamara MG, Lopes A, Wasan H, Malka D, Goldstein D, Shannon J, et al. Landmark survival analysis and impact of anatomic site of origin in prospective clinical trials of biliary tract cancer. *J Hepatol*. 2020;73(5):1109–17.
31. Rimland CA, Tilson SG, Morell CM, Tomaz RA, Lu WY, Adams SE, et al. Regional differences in human biliary tissues and corresponding in Vitro-Derived organoids. *Hepatology*. 2021;73(1):247–67.
32. Valle JW, Lamarca A, Goyal L, Barriuso J, Zhu AX. New horizons for precision medicine in biliary tract cancers. *Cancer Discov*. 2017;7(9):943–62.
33. Song Y, Boerner T, Drill E, Shin P, Kumar S, Sigel C et al. A novel approach to quantify heterogeneity of intrahepatic cholangiocarcinoma: the Hidden-Genome classifier. *Clin Cancer Res* 2024.
34. Spencer K, Pappas L, Baiev I, Maurer J, Bocobo AG, Zhang K, et al. Molecular profiling and treatment pattern differences between intrahepatic and extrahepatic cholangiocarcinoma. *J Natl Cancer Inst*. 2023;115(7):870–80.
35. Sasaki M, Ikeda H, Yamaguchi J, Miyakoshi M, Sato Y, Nakanuma Y. Bile ductular cells undergoing cellular senescence increase in chronic liver diseases along with fibrous progression. *Am J Clin Pathol*. 2010;133(2):212–23.
36. Cogliati B, Yashaswini CN, Wang S, Sia D, Friedman SL. Friend or foe? The elusive role of hepatic stellate cells in liver cancer. *Nat Rev Gastroenterol Hepatol*. 2023;20(10):647–61.
37. Gilson E, Soubeyran P, Solary E. Targeting senescence for Next-Generation Cancer treatments. *Cancer Discov*. 2024;14(4):635–8.
38. Sanchez-Danes A, Blanpain C. Deciphering the cells of origin of squamous cell carcinomas. *Nat Rev Cancer*. 2018;18(9):549–61.
39. Gardner EE, Earlie EM, Li K, Thomas J, Hubisz MJ, Stein BD, et al. Lineage-specific intolerance to oncogenic drivers restricts histological transformation. *Science*. 2024;383(6683):eadj1415.
40. Cheung KJ, Gabrielson E, Werb Z, Ewald AJ. Collective invasion in breast cancer requires a conserved basal epithelial program. *Cell*. 2013;155(7):1639–51.
41. Moffitt RA, Marayati R, Flate EL, Volmar KE, Loeza SG, Hoadley KA, et al. Virtual microdissection identifies distinct tumor- and stroma-specific subtypes of pancreatic ductal adenocarcinoma. *Nat Genet*. 2015;47(10):1168–78.
42. Inayatullah M, Mahesh A, Turnbull AK, Dixon JM, Natrajan R, Tiwari VK. Basal-epithelial subpopulations underlie and predict chemotherapy resistance in triple-negative breast cancer. *EMBO Mol Med*. 2024;16(4):823–53.
43. Pitzen SP, Dehm SM. Basal epithelial cells in prostate development, tumorigenesis, and cancer progression. *Cell Cycle*. 2023;22(11):1303–18.
44. Russo M, Chen M, Mariella E, Peng H, Rehman SK, Sancho E, et al. Cancer drug-tolerant persister cells: from biological questions to clinical opportunities. *Nat Rev Cancer*. 2024;24(10):694–717.
45. Locke M. *Developmental Biology: Academic*; 2014.
46. Patel AS, Yanai L. A developmental constraint model of cancer cell States and tumor heterogeneity. *Cell*. 2024;187(12):2907–18.
47. Kang M, Kim NR, Chung DH, Cho HY, Park YH. Squamous cell carcinoma of the extrahepatic common hepatic duct. *J Pathol Transl Med*. 2019;53(2):112–8.
48. Zhang Y, Bailey D, Yang P, Kim E, Que J. The development and stem cells of the esophagus. *Development* 2021;148(6).
49. Tong X, Patel AS, Kim E, Li H, Chen Y, Li S, et al. Adeno-to-squamous transition drives resistance to KRAS inhibition in LKB1 mutant lung cancer. *Cancer Cell*. 2024;42(3):413–e428417.
50. Wang M, Chen X, Tan P, Wang Y, Pan X, Lin T, et al. Acquired semi-squamatization during chemotherapy suggests differentiation as a therapeutic strategy for bladder cancer. *Cancer Cell*. 2022;40(9):1044–e10591048.
51. van der Meer JH, van der Poll T, van't Veer C. TAM receptors, Gas6, and protein S: roles in inflammation and hemostasis. *Blood*. 2014;123(16):2460–9.
52. Peacock AJ, Dawes KE, Shock A, Gray AJ, Reeves JT, Laurent GJ. Endothelin-1 and endothelin-3 induce chemotaxis and replication of pulmonary artery fibroblasts. *Am J Respir Cell Mol Biol*. 1992;7(5):492–9.
53. Avolio E, Campagnolo P, Katare R, Madeddu P. The role of cardiac pericytes in health and disease: therapeutic targets for myocardial infarction. *Nat Rev Cardiol*. 2024;21(2):106–18.
54. Banales JM, Cardinale V, Carpino G, Marzioni M, Andersen JB, Invernizzi P, et al. Expert consensus document: cholangiocarcinoma: current knowledge and future perspectives consensus statement from the European network for the study of cholangiocarcinoma (ENS-CCA). *Nat Rev Gastroenterol Hepatol*. 2016;13(5):261–80.
55. Wu X, Dao Thi VL, Huang Y, Billerbeck E, Saha D, Hoffmann HH, et al. Intrinsic immunity shapes viral resistance of stem cells. *Cell*. 2018;172(3):423–e438425.
56. Sato T, Ishikawa S, Asano J, Yamamoto H, Fujii M, Sato T, et al. Regulated IFN signalling preserves the stemness of intestinal stem cells by restricting differentiation into secretory-cell lineages. *Nat Cell Biol*. 2020;22(8):919–26.
57. Musella M, Guarracino A, Manduca N, Galassi C, Ruggiero E, Potenza A, et al. Type I IFNs promote cancer cell stemness by triggering the epigenetic regulator KDM1B. *Nat Immunol*. 2022;23(9):1379–92.
58. Hajishengallis G, Netea MG, Chavakis T. Trained immunity in chronic inflammatory diseases and cancer. *Nat Rev Immunol* 2025.
59. Wu MS, Kuo YP, Lo YC, Tsai DJ, Lai CY, Chuang TH, et al. Type I interferon signaling accelerates liver regeneration by metabolic modulation in noninfectious conditions. *Am J Pathol*. 2021;191(6):1036–48.
60. Ronca V, Gerussi A, Collins P, Parente A, Oo YH, Invernizzi P. The liver as a central hub of the immune system: pathophysiological implications. *Physiol Rev*. 2025;105(2):493–539.
61. Takii Y, Nakamura M, Ito M, Yokoyama T, Komori A, Shimizu-Yoshida Y, et al. Enhanced expression of type I interferon and toll-like receptor-3 in primary biliary cirrhosis. *Lab Invest*. 2005;85(7):908–20.
62. Alpini G, Glaser S, Robertson W, Phinizy JL, Rodgers RE, Caligiuri A, et al. Bile acids stimulate proliferative and secretory events in large but not small cholangiocytes. *Am J Physiol*. 1997;273(2 Pt 1):G518–529.
63. LeSage GD, Glaser SS, Marucci L, Benedetto A, Phinizy JL, Rodgers R, et al. Acute carbon tetrachloride feeding induces damage of large but not small cholangiocytes from BDL rat liver. *Am J Physiol*. 1999;276(5):G1289–1301.
64. Alpini G, Glaser SS, Ueno Y, Pham L, Podila PV, Caligiuri A, et al. Heterogeneity of the proliferative capacity of rat cholangiocytes after bile duct ligation. *Am J Physiol*. 1998;274(4):G767–775.
65. Holicek P, Guilbaud E, Klapp V, Truxova I, Spisek R, Galluzzi L, et al. Type I interferon and cancer. *Immunol Rev*. 2024;321(1):115–27.
66. Zitvogel L, Galluzzi L, Kepp O, Smyth MJ, Kroemer G. Type I interferons in anticancer immunity. *Nat Rev Immunol*. 2015;15(7):405–14.

67. Saab M, Mestivier D, Sohrabi M, Rodriguez C, Khonsari MR, Faraji A, et al. Characterization of biliary microbiota dysbiosis in extrahepatic cholangiocarcinoma. *PLoS ONE*. 2021;16(3):e0247798.
68. Winkler ES, Shrihari S, Hykes BL Jr., Handley SA, Andhey PS, Huang YS, et al. The intestinal Microbiome restricts alphavirus infection and dissemination through a bile acid-Type I IFN signaling axis. *Cell*. 2020;182(4):901–e918918.
69. Singh S, Lian Q, Budiman T, Taketo MM, Simons BD, Gupta V. Heterogeneous murine peribiliary glands orchestrate compartmentalized epithelial renewal. *Dev Cell*. 2023;58(23):2732–e27452735.
70. Ablasser A, Chen ZJ. cGAS in action: expanding roles in immunity and inflammation. *Science* 2019;363(6431).
71. Bowlus CL, Arrive L, Bergquist A, Deneau M, Forman L, Ilyas SI, et al. AASLD practice guidance on primary sclerosing cholangitis and cholangiocarcinoma. *Hepatology*. 2023;77(2):659–702.
72. Guo XJ, Lu JC, Zeng HY, Zhou R, Sun QM, Yang GH, et al. CTLA-4 synergizes with PD1/PD-L1 in the inhibitory tumor microenvironment of intrahepatic cholangiocarcinoma. *Front Immunol*. 2021;12:705378.
73. Galassi C, Chan TA, Vitale I, Galluzzi L. The hallmarks of cancer immune evasion. *Cancer Cell*. 2024;42(11):1825–63.
74. Wardlaw CP, Petrini JHJ. ISG15 conjugation to proteins on nascent DNA mitigates DNA replication stress. *Nat Commun*. 2022;13(1):5971.
75. Wang X, Fu J. [The biliary ecosystem: a holistic perspective on critical scientific issues regarding biliary tract surgeries and diseases]. *Zhonghua Wai Ke Za Zhi*. 2025;63(1):39–44.

### Publisher's note

Springer Nature remains neutral with regard to jurisdictional claims in published maps and institutional affiliations.